24th INTERNATIONAL CONGRESS ON SOUND AND VIBRATION
23–27 July 2017, London

ICSV24
23-27JULY 2017
LONDON CALLING

OPTIMISING THE ACOUSTICS OF SHORT CIRCULAR HOLES WITH MEAN FLOW

Holly G. Johnson and Aimee S. Morgans
Imperial College London, Department of Mechanical Engineering, South Kensington, London, UK
email: holly.johnson@imperial.ac.uk

Short circular holes with a high Reynolds mean flow passing through them are a common occurrence in applications such as Helmholtz resonators, perforated plates or liners and fuel injectors. The acoustic response of such holes has been shown to be strongly dependent on the path followed by the vorticity which is shed at the hole inlet and convected downstream to form a vortex sheet. Coupling between this vorticity and the acoustic waves has the potential either to absorb or to generate acoustic energy in the low frequency region. A semi-analytical model based on Green's function method (*The acoustics of short circular holes opening to confined and unconfined spaces*, Yang & Morgans, Journal of Sound and Vibration, 2017) is combined with a gradient-based optimisation technique to determine the optimal vortex sheet shapes for absorption or amplification of noise. As the shape of the vortex sheet depends directly on the geometry of the hole inlet, finding the optimal shape provides information on the geometry required to achieve the desired acoustic effect.

Keywords: Hole acoustics, Optimisation, Analytical model

1. Introduction

In many practical applications such as internal combustion or aero-engines, acoustic damping is achieved using perforated liners with a high Reynolds number mean flow passing through. The acoustic response of short holes with mean flow is also relevant to many other applications such as Helmholtz resonators and fuel injectors. The damping is due to the conversion of acoustic energy into sound-induced vortex shedding [1] at the hole inlet, resulting in significant attenuation at low frequencies.

The acoustic response of an infinitely short hole opening to semi-infinitely large spaces on both sides was first studied by Howe [2] who determined an analytical expression of the Rayleigh conductivity of the hole. In this model the vortex sheet formed at the hole inlet is assumed to be straight and cylindrical. For practical applications, an additional mass inertial term can be added to Howe's model to account for a small hole length and the consequent contraction of the vortex sheet as it passes through the hole. Other methods for predicting the impedance of a short hole include that of Bellucci et al.[3] which is founded on the conservation of momentum of a one-dimensional compressible flow across the hole.

However, experimental results [4, 5] have shown that when the hole length is of the same order as the diameter, the acoustic impedance is somewhat different from that predicted by either of these models. In particular, with growing Strouhal number the resistance of the hole decreases to the point where it can become negative, indicating that the hole is no longer absorbing but generating acoustic energy, whereas Howe and Bellucci's models predict only absorption. The generation of sound is due

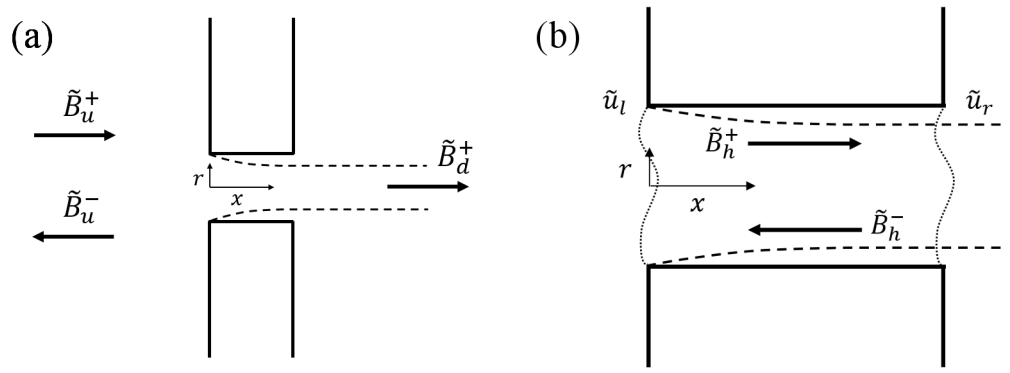

Figure 1: (a) Schematic of the short circular hole opening to semi-infinitely large spaces on either side, the shed vortex sheet and the relevant acoustic waves ($\tilde{B}$ is the Fourier amplitude of the stagnation enthalpy oscillations defined in Eq. (3)); (b) Schematic of the velocity oscillations at the hole inlet and outlet and the relevant acoustic waves. Please note the diagrams are not to scale.

to a self-sustained oscillation mechanism which has previously been well documented [6, 7, 8, 9]. Vorticity shed at the hole inlet is advected downstream and affects the sound radiation at the hole outlet. Reflected waves propagate upstream and, together with the oscillations generated directly by the vortex sheet, influence the vortex shedding at the inlet edge. Jing & Sun [4] developed a numerical model taking into account the hole length and using experimental measurements of the geometry of the vortex sheet. Their numerical results compared well with their experimental data. Su et al. [5] carried out experiments and CFD for holes of varying length which compared well. Once again this work shows that only by taking into account the exact shape of the vortex sheet can an accurate prediction of the acoustic response be made. However, as computational methods remain expensive and time-consuming, Yang & Morgans [10, 11] developed an analytical model based on Green's function method which predicts the acoustic response of finite length holes open to unconfined or confined spaces on either side. The results provided by this model are consistent with the experimental, numerical and CFD results of [4, 5]. Yang & Morgans show that both the vortex sheet contraction coefficient and the shape of the sheet near the inlet edge can influence greatly the vortex shedding and therefore the hole impedance.

This work aims to combine a gradient-based optimisation technique with the analytical model developed by Yang & Morgans in order to determine the vortex sheet shapes providing maximal sound absorption and generation. Depending on the application, this information will indicate the optimal hole inlet edge geometry (which dictates the vortex sheet shape for a given Reynolds number) to use in order to attain the desired acoustic effect. This paper is organised as follows. Firstly, the method behind the semi-analytical model of Yang & Morgans [10, 11] is outlined to provide a basic grasp of the model. Secondly, the optimisation approach is detailed and elements of validation are presented. Finally the preliminary results obtained using this method are discussed.

2. The semi-analytical acoustic model

We consider a short circular hole of radius R and length $L = R$, open to semi-infinite spaces on both sides (see Fig 1 (a)). A high Reynolds number mean flow of velocity $\bar{u}$ assumed to be parallel to the axial direction (x) passes through the hole, giving a mean Mach number $\bar{M} = \bar{u}/c$ with c the sound speed. A low-frequency incoming acoustic wave of sufficiently large wavelength to be considered as a planar wave causes the shedding of oscillating vortices with matching frequency from the hole inlet edge. The vorticity is advected through the hole and downstream to form a vortex sheet as shown in Fig 1 (a) (the dotted line denotes the vortex sheet). Reflected and transmitted waves

are generated as the incident wave encounters the hole inlet and outlet (a detailed schematic of the physics inside the hole is provided in Fig 1 (b)). Oscillations reflected at the hole outlet affect the vortex shedding process at the inlet. Additionally the vortex sheet directly induces oscillations at the hole inlet which in turn affect the vortex shedding. The main features of the model are outlined in the following paragraphs; the reader is referred to [10] and [11] for further details.

As the effect of viscosity can be neglected apart from close to the hole inlet, volume forces are assumed negligible and the flow isentropic, the momentum equation can be written in Crocco's form [12]:

$$\frac{\partial \boldsymbol{u}}{\partial t} + \nabla B = -\left(\boldsymbol{\omega} \times \boldsymbol{u}\right) \tag{1}$$

where B is the stagnation enthalpy, $\boldsymbol{u}$ is the velocity and $\boldsymbol{\omega}$ the vorticity. The conservation of mass gives:

$$\frac{\partial \rho}{\partial t} + \boldsymbol{u} \cdot \nabla \rho + \rho \nabla \cdot \boldsymbol{u} = 0 \tag{2}$$

with ρ the density. By combining the two equations, decomposing all parameters into mean and oscillating parts (for example, $\rho = \bar{\rho} + \rho'$) and considering first order fluctuations only, a convected wave equation is reached:

$$\left(\frac{1}{\bar{c}}\left(\frac{\partial}{\partial t} + \bar{u}\frac{\partial}{\partial x}\right)^2 - \nabla^2\right) B' = \nabla \cdot \left(\boldsymbol{\omega}' \times \boldsymbol{u_c}\right) \tag{3}$$

where $\boldsymbol{u_c}$ is the vortex convection velocity, taken to be equal to the mean velocity in the hole [13, 14, 4]. This equation is solved by introducing a Green's function $G\left(\boldsymbol{x}, t|\boldsymbol{y}, \tau\right)$ which, when defined in the frequency domain as $\tilde{G}\left(\boldsymbol{x}, \boldsymbol{y}, \omega\right)$, satisfies:

$$\left(\frac{1}{\bar{c}}\left(-i\omega + \bar{u}\frac{\partial}{\partial x}\right)^2 - \nabla^2\right) \tilde{G} = \delta\left(\boldsymbol{x} - \boldsymbol{y}\right) \tag{4}$$

with δ the Dirac function, $\boldsymbol{x}$ the space in which the wave equation is solved and $\boldsymbol{y}$ the acoustic source location. The problem is then separated into three distinct spaces: upstream of the hole, inside the hole and downstream of the hole (the subscripts $[]_u$, $[]_h$ and $[]_d$ denote the properties of these spaces respectively). The Green's function satisfying Eq. (4) for each space is determined by including appropriate boundary conditions and taking into account all the relevant acoustic sources. For example, the boundary conditions for the upstream region are that the velocity oscillations just upstream of the hole inlet should be zero ($d\tilde{G}_u/dx(x = 0^-) = 0$) and only outgoing waves propagate infinitely far away from the inlet. Upstream of the hole the sources are the incident wave and the velocity oscillation at the hole inlet. Similar boundary conditions are applied downstream and the sources in this region are the velocity oscillations at the hole outlet and the vortex sheet. Inside the hole, two Green's functions $\tilde{G}_h^l$ and $\tilde{G}_h^r$ are used for simplicity as explained in [10]. The boundary conditions are zero-radial velocity on the hole's inner surface ($d\tilde{G}_h^{l,r}(r = R) = 0$), $d\tilde{G}_u^l/dx(x = 0^+) = 0$, $d\tilde{G}_u^r/dx(x = L^-) = 0$ and only outward waves propagating at the right (resp. left) boundary. Using this method, the stagnation enthalpy oscillations in the three spaces can be obtained.

To calculate the vortex-induced oscillations, the vortex sheet is discretised into N_v short cone rings. The velocity oscillations at the hole inlet $\tilde{u}_l$ and outlet $\tilde{u}_r$ are expressed as sums of Bessel functions (e.g $\tilde{u}_l = \sum_{m=0}^{+\infty} U_{lm} J_0\left(j_m r/R\right)$, with J_0 the Bessel function of order 0 and j_m the mth zero of J_1) and are calculated by applying stagnation enthalpy continuity across the hole inlet and outlet interfaces (the series are truncated at the Mth term). The Kutta condition is applied at the hole inlet edge to determine the vortex sheet strength σ. Finally the acoustic response of the hole can be calculated. For example, the Rayleigh conductivity of the hole is:

$$K_R = -\frac{i\omega\bar{\rho}\tilde{Q}}{\Delta\tilde{p}} \tag{5}$$

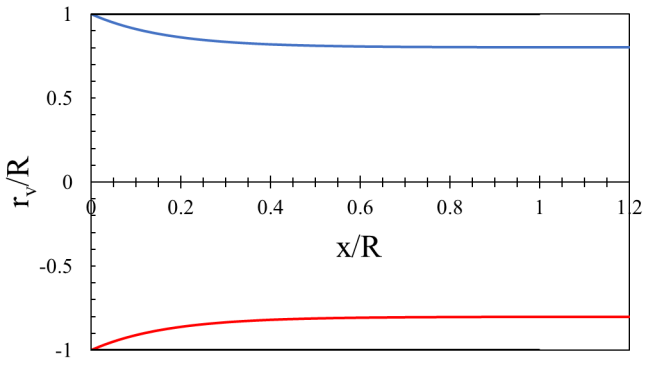

Figure 2: Illustration of the analytical definition (Eq. (6)) of the vortex sheet shape with $a = 0.2$ and $b = 6$ (in blue) and its symmetric counterpart (in red).

with ω the frequency, $\tilde{Q} = U_{l0}\pi R^2$ the volume flux oscillation through the hole, U_{l0} the first component of the velocity oscillations at the hole inlet and $\Delta\tilde{p}/\bar{\rho} = 2\tilde{B}^+_{u0}$ the pressure difference across the hole. As the whole system is linear, the amplitude of the incoming wave $\tilde{B}^+_{u0} = 1$ can be taken arbitrarily. The frequency is normalised by introducing the Strouhal number $St = \omega R/u_c$.

3. Optimisation of the vortex sheet shape

The objective of this work is to determine the optimal vortex sheet shape providing the desired acoustic response of the hole. The vortex sheet shape is defined analytically by:

$$\frac{r_v}{R} = 1 - a\left(1 - e^{-bx/R}\right) \tag{6}$$

with r_v the radial position of the vortex sheet at the axial coordinate x. An example of a vortex sheet described by this expression is provided in Fig. 2. The vortex sheet is assumed to be fully contracted, therefore straight and aligned with the hole axis, when it reaches the hole outlet. The optimisation problem has two control variables: the vortex sheet contraction coefficient (controlled through a) and the initial slope at the inlet edge (controlled through b). It is shown [11] that the acoustic energy absorbed by the hole is directly related to the hole resistance Δ_R: the imaginary part of the Rayleigh conductivity $K_R = 2R\left(\Gamma_R - i\Delta_R\right)$. When the resistance becomes negative, acoustic energy is being generated by the flow through the hole. This quantity is chosen to be the cost functional $\mathcal{J}$, that is the variable which will be optimised. Using Eq. (5) and the expressions of the volume flux oscillation and the pressure difference, the expression of this cost function is:

$$\mathcal{J} = \Delta_R = \frac{\pi R}{4}\Im\left(i\omega U_{l0}\right) \tag{7}$$

where $\Im$ denotes the imaginary part.

3.1 Optimisation method

A Lagrange multiplier technique [15] with a gradient-based update method (such as that used by Marquet et al. [16]) is applied to solve the optimisation problem. The Lagrange function is defined as:

$$\mathcal{L}\left(\boldsymbol{q}, \boldsymbol{g}, \boldsymbol{\lambda}\right) = \mathcal{J}\left(\boldsymbol{q}\right) - \boldsymbol{\lambda} \cdot \boldsymbol{F}\left(\boldsymbol{q}, \boldsymbol{g}\right) \tag{8}$$

with $\boldsymbol{g} = (a, b)^T$ the control variables, $\boldsymbol{q}$ the state variables, $\boldsymbol{\lambda}$ the Lagrange multiplier vector and $\boldsymbol{F}\left(\boldsymbol{q}, \boldsymbol{g}\right) = \boldsymbol{0}$ the state equation. There are seven state variables: $\boldsymbol{q} = \left(U_{l0}, \sigma, Y_d, Y_{hl}, Y_{hr}, S_{dl}, S_{dr}\right)^T$ with Y_d relating to the acoustic contribution of the straight vortex sheet downstream of the hole, and

Y_{hl} and Y_{hr} the overall contributions of the vortex sheet inside the hole on the hole inlet and outlet stagnation enthalpy oscillations respectively. As defined in Eqs. (22, 23) of Yang & Morgans [10], S_{dl} and S_{dr} relate to the direct contributions of the discretised vortex sheet to the hole inlet and outlet stagnation enthalpy oscillations respectively. Setting to zero the variation of the Lagrange function with respect to the state variables gives the adjoint equation (9).

$$\frac{\partial \mathcal{L}}{\partial \boldsymbol{q}} = \mathbf{0} \quad \Rightarrow \quad \frac{\partial \mathcal{J}}{\partial \boldsymbol{q}} = \boldsymbol{\lambda} \cdot \frac{\partial \boldsymbol{F}}{\partial \boldsymbol{q}} \tag{9}$$

The components of the Lagrange multiplier vector are determined by solving the adjoint equation. The steepest descent direction is obtained by deriving the Lagrange function with respect to the control variables:

$$\frac{\partial \mathcal{L}}{\partial \boldsymbol{g}} = \frac{\partial \mathcal{J}}{\partial \boldsymbol{g}} - \boldsymbol{\lambda} \cdot \frac{\partial \boldsymbol{F}}{\partial \boldsymbol{g}} = -\boldsymbol{\lambda} \cdot \frac{\partial \boldsymbol{F}}{\partial \boldsymbol{g}} \tag{10}$$

The optimisation follows an iterative procedure providing convergence to the optimal state $\boldsymbol{g}^* = (a^*, b^*)^T$:

(1) Initial guess of control variables $\boldsymbol{g}^0 = (a^0, b^0)^T$
(2) Solve the state equation $\boldsymbol{F}(\boldsymbol{q}, \boldsymbol{g}) = \mathbf{0}$ to determine the state variables $\boldsymbol{q}$
(3) Solve the adjoint equation (9) to determine the Lagrange multiplier vector $\boldsymbol{\lambda}$
(4) Deduce the steepest descent direction (10) and update the control variables
(5) Loop from (2) to (4) until convergence

The control vector is updated using a steepest descent method: $\boldsymbol{g}^{i+1} = \boldsymbol{g}^i + \alpha^i \partial \mathcal{L} / \partial \boldsymbol{g}$, with α^i a small step size. The convergence towards the optimal solution is monitored through the relative increment of the cost function with respect to the previous iteration:

$$e = \frac{\mathcal{J}^{i+1} - \mathcal{J}^i}{\mathcal{J}^{i+1}} \tag{11}$$

The optimisation is considered to be converged when $e < 10^{-6}$. Another convergence criterion is that the norm of the steepest descent direction tends to zero. This criterion is also checked before concluding the optimisation procedure.

Note that the procedure described above will search for a local or global minimum of the cost functional $\mathcal{J}$. The resulting optimal solution (a^*, b^*) will provide the vortex sheet shape leading to the least acoustic energy absorption. Obtaining the optimal solution corresponding to a maximisation of acoustic damping is achieved simply by replacing the cost function by $-\mathcal{J}$.

In order to guarantee physically acceptable results, the following constraints are imposed at each iteration i. The contraction coefficient a must satisfy $0 < a < 1$, the initial slope $b > 0$, and finally the vortex sheet must be fully converged when reaching the hole outlet $dr/dx\,(x = L) < 0.01R$. The conditions are imposed using a logarithmic barrier method. The Lagrange function becomes:

$$\mathcal{L}(\boldsymbol{q}, \boldsymbol{g}, \boldsymbol{\lambda}) = \mathcal{J}(\boldsymbol{q}) - \boldsymbol{\lambda} \cdot \boldsymbol{F}(\boldsymbol{q}, \boldsymbol{g}) - \mu \sum_{j=1}^{4} \log c_j(\boldsymbol{g}) \tag{12}$$

with $\mu > 0$ a barrier parameter, and $c_j \geq 0, j = 1, ...4$ the inequality constraints defined as: $c_1 = a - \epsilon$, $c_2 = 1 - a - \epsilon$, $c_3 = b - \epsilon$ and $c_4 = 0.01R - abe^{-bL/R}$ where $\epsilon > 0$ is a small buffer parameter ($\epsilon << 1$). As the constraints refer specifically to the control parameters, only the steepest descent direction is impacted:

$$\frac{\partial \mathcal{L}}{\partial \boldsymbol{g}} = -\boldsymbol{\lambda} \cdot \frac{\partial \boldsymbol{F}}{\partial \boldsymbol{g}} - \mu \sum_{j=1}^{4} \frac{1}{c_j(\boldsymbol{g})} \tag{13}$$

The barrier parameter μ is first set to 1 and then progressively diminished. As $\mu \to 0$ the minimiser of the Lagrange functional tends towards the minimiser of the cost function. This practice is particularly necessary in cases such as that described in Section 3.2 where the solution is close to one of the boundaries imposed on the control variables.

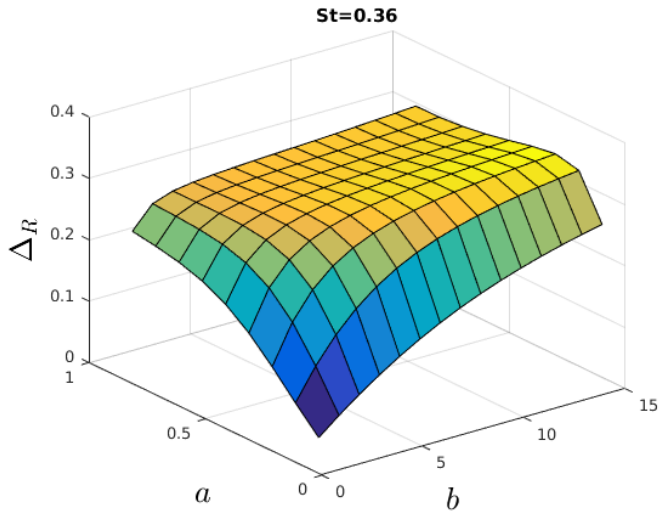

Figure 3: Mapping of the hole's acoustic resistance Δ_R as a function of the control parameters a and b for $St = 0.36$.

3.2 Validation

As, to our knowledge, no such optimisation study has been carried out before, no comparisons with existing results can be made. Accordingly, an alternative method to validate the optimisation code has been devised. The semi-analytical model of Yang & Morgans was validated by comparing results with experimental and computational data [5]. Using this model, a sweep of the control parameter field provides the hole resistance for each (a,b) for a given Strouhal number. We consider the following case: $R = 6.10^{-3}$ m, $\bar{M} = 6.2.10^{-2}$ at room temperature $T = 290$ K and pressure $P = 10^5$ Pa. An example of a mapping obtained using this method is shown in Fig. 3 for a Strouhal number of $St = 0.36$. It is clear that a global minimum of the resistance can be attained in the region $(a, b) \approx (0, 0)$. The optimisation code minimising the resistance gives an optimal state of $(a^*, b^*) = (1.10^{-15}, 1.2.10^{-4})$, which agrees well with the mapping of Fig. 3.

The robustness of the optimisation tool is tested by starting from varied initial guesses (a^0, b^0) as shown in Fig. 4 (a), all the tests converge on the same point within five iterations and yield the same minimum resistance $\Delta_R^* = 1.26.10^{-3}$. Finally, for each optimisation, the values of the relative increment of the resistance between consecutive iterations e and the components of the steepest descent direction $\partial\mathcal{L}/\partial a$ and $\partial\mathcal{L}/\partial b$ are monitored to check the quality of the convergence to the optimal state. Figure 4 (b) gives these values evolving through the iterative process for the calculation beginning with $(a^0, b^0) = (0.8, 3)$. Within ten iterations e drops below 10^{-10} and the gradients reach 10^{-6} which are satisfactory convergence conditions. Many similar validation analyses are carried out in order to ensure the code functions correctly for all Strouhal numbers and initial guesses.

4. Analysis of preliminary results

Firstly, based on the result presented in the validation phase, it seems that for low frequencies, minimal acoustic damping occurs when the vortex sheet is straight. Although in application, it is physically impossible for there to be no contraction at all, adaptation of the shape of the hole inlet edge could lead to a minimally contracted vortex sheet. As the intention of many applications is to reduce noise, this case would represent a 'worst case scenario' providing the smallest possible absorption and the conditions that induce it.

Secondly, it appears that at low frequencies, the hole resistance can tend to zero but does not

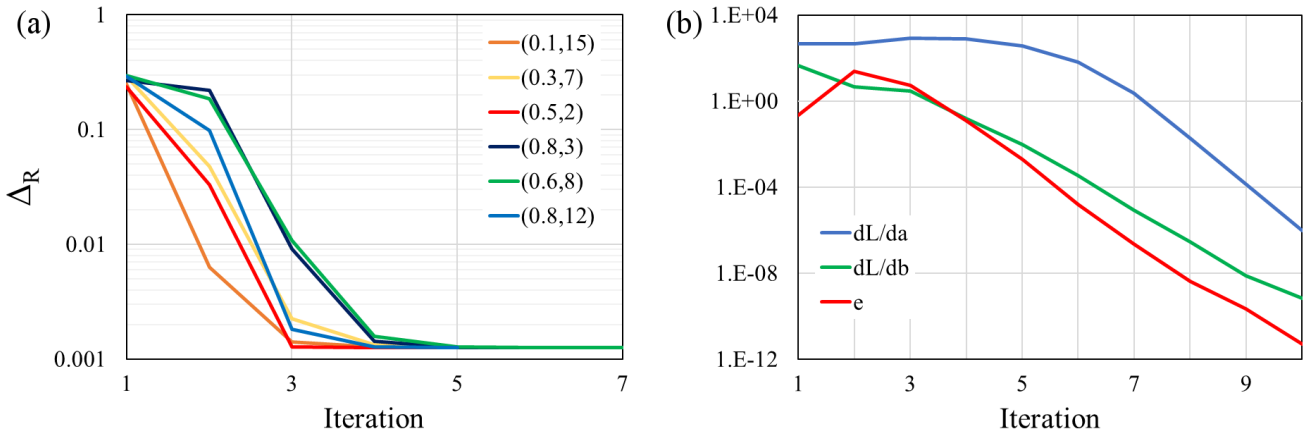

Figure 4: (a) Convergence of the acoustic resistance Δ_R of the hole towards the minimal value Δ_R^* for varying initial guesses (a^0, b^0); (b) Evolution throughout the optimisation of the relative increment of the resistance between consecutive iterations e and the components of the steepest descent direction $\partial\mathcal{L}/\partial a$ and $\partial\mathcal{L}/\partial b$ for the case of initial guess $(a^0, b^0) = (0.8, 3)$.

become negative, ruling out the potential generation of noise through the feedback mechanism. This is consistent with the experimental and numerical findings described in the introduction. Additional results for other Strouhal numbers will confirm that in general this is the case for low frequencies and perhaps provide a critical frequency range within which the resistance can become negative.

REFERENCES

1. Dupere, I. and Dowling, A. The absorption of sound near abrupt axisymmetric area expansions, *Journal of sound and vibration*, **239** (4), 709–730, (2001).

2. Howe, M. On the theory of unsteady high Reynolds number flow through a circular aperture, *Proceedings of the Royal Society of London A: Mathematical, Physical and Engineering Sciences*, vol. 366, pp. 205–223, The Royal Society, (1979).

3. Bellucci V., P. C. O., Flohr P. and F., M. On the use of Helmholtz resonators for damping acoustic pulsations in industrial gas turbines, *Journal of Engineering for Gas Turbines and Power*, **126** (2), 271–275, (2004).

4. Jing, X. and Sun, X. Effect of plate thickness on impedance of perforated plates with bias flow, *AIAA journal*, **38** (9), 1573–1578, (2000).

5. Su, J., Rupp, J., Garmory, A. and Carrotte, J. F. Measurements and computational fluid dynamics predictions of the acoustic impedance of orifices, *Journal of Sound and Vibration*, **352**, 174–191, (2015).

6. Rockwell, D. and Naudascher, E. Self-sustained oscillations of impinging free shear layers, *Annual Review of Fluid Mechanics*, **11** (1), 67–94, (1979).

7. Howe, M. S., *Hydrodynamics and sound*, Cambridge University Press (2006).

8. Testud, P. H., Aurégan, Y., Moussou, P. and Hirschberg, A. The whistling potentiality of an orifice in a confined flow using an energetic criterion, *Journal of Sound and Vibration*, **325** (4), 769–780, (2009).

9. Kierkegaard, A., Allam, S., Efraimsson, G. and Åbom, M. Simulations of whistling and the whistling potentiality of an in-duct orifice with linear aeroacoustics, *Journal of sound and vibration*, **331** (5), 1084–1096, (2012).

10. Yang, D. and Morgans, A. S. A semi-analytical model for the acoustic impedance of finite length circular holes with mean flow, *Journal of Sound and Vibration*, **384**, 294–311, (2016).

11. Yang, D. and Morgans, A. S. The acoustics of short circular holes opening to confined and unconfined spaces, *Journal of Sound and Vibration*, **393**, 41–61, (2017).

12. Howe, M. S., *Acoustics of fluid-structure interactions*, Cambridge university press (1998).

13. Hughes, I. J. and Dowling, A. P. The absorption of sound by perforated linings, *Journal of Fluid Mechanics*, **218**, 299–335, (1990).

14. Eldredge, J. D. and Dowling, A. P. The absorption of axial acoustic waves by a perforated liner with bias flow, *Journal of Fluid Mechanics*, **485**, 307–335, (2003).

15. Zuccher, S., Luchini, P. and Bottaro, A. Algebraic growth in a Blasius boundary layer: optimal and robust control by mean suction in the nonlinear regime, *Journal of Fluid Mechanics*, **513**, 135–160, (2004).

16. Marquet, O., Sipp, D. and Jacquin, L. Sensitivity analysis and passive control of cylinder flow, *Journal of Fluid Mechanics*, **615**, 221–252, (2008).